Journal of Power Sources 239 (2013) 393–398

Contents lists available at SciVerse ScienceDirect

Journal of Power Sources

journal homepage: www.elsevier.com/locate/jpowsour

Short communication

ZnO-template-mediated synthesis of three-dimensional coral-like MnO_2 nanostructure for supercapacitors

Yong Zhao [a], Peng Jiang [a,*], Si-Shen Xie [b,*]

[a] National Center for Nanoscience and Technology (NCNST), Beijing 100190, PR China
[b] Institute of Physics, Beijing Natl Lab Condensed Matter Phys, Chinese Academy of Sciences (CAS), Beijing 100190, PR China

HIGHLIGHTS

- A novel three-dimensional coral-like MnO_2 thin-film has been prepared directly on stainless steel substrate.
- The synthesis method is a quite simple and low-cost one-step ZnO nanorod arrays-mediated strategy.
- The coral-like MnO_2 is constituted by 2–5 nm birnessite-MnO_2 nanoparticles, exhibiting improved electrochemical performance.

GRAPHICAL ABSTRACT

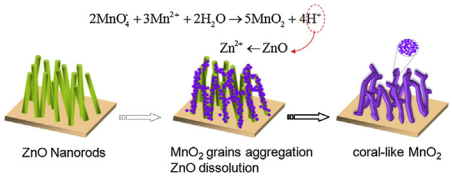

ARTICLE INFO

Article history:
Received 9 January 2013
Received in revised form
19 March 2013
Accepted 29 March 2013
Available online 8 April 2013

Keywords:
Manganese dioxide
Zinc oxide
Nanowire
Template method
Supercapacitor

ABSTRACT

A kind of coral-like porous MnO_2 nanostructure film has been formed on stainless steel using a facile ZnO-nanorod-array-mediated technique by a hydrothermal method. Thus-constructed electrode materials for supercapacitors exhibit a high specific capacitance of 221 F g^{-1} at 0.5 A g^{-1} and excellent cycle ability with 86% retention after 3000 cycles at 5 A g^{-1}. The excellent electrochemical performance of the electrode materials is considered to be originated from the porous and hierarchical three-dimensional MnO_2 nanostructure on the conductive stainless steel substrate.

1. Introduction

Supercapacitors, also known as electrochemical capacitors, have recently attracted intense interests due to their high power density, long cycle lifetime and safe operation for promising applications from portable electronics to next-generation hybrid electric vehicles [1,2]. Typical electrode materials widely used for supercapacitors include carbon materials, transition metal oxides and conductive polymers. Among the available electrode materials, MnO_2 has been reckoned as one of the most attractive candidates owing to its low cost, environmentally benign nature and high theoretical specific capacitance [3]. However, MnO_2 bulk materials usually exhibit low specific capacitances due to its intrinsic poor electrical conductivity, which has limited its application as electrode material for effective energy storage [4].

To improve the electrochemical performance, MnO_2 nanostructures with desirable morphologies and crystal structures have been extensively investigated recently. Especially, three-dimensional (3D) porous MnO_2 thin films have gained more and more attention because of their remarkable advantages over the bulk counterparts such as higher surface area and less dead volume [5,6]. More importantly, the thin films can be directly deposited on

* Corresponding authors. Tel.: +86 10 82545549; fax: +86 10 62656765.
E-mail addresses: pjiang@nanoctr.cn (P. Jiang), ssxie@aphy.iphy.ac.cn (S.-S. Xie).

0378-7753/$ – see front matter © 2013 Elsevier B.V. All rights reserved.
http://dx.doi.org/10.1016/j.jpowsour.2013.03.176

conductive substrates used as electrodes without adding binders and conductive additives, which can effectively reduce the total weight and cost for industrial production. In general, the 3D MnO_2 nanostructure thin films are fabricated by using various templates such as anodic aluminium oxide (AAO) and polystyrene spheres (PS) [7–9]. However, these templates suffer from high cost and complicate removal process through acid or base etching and calcinations [10]. Therefore, a great challenge based on the consideration is to utilize possible low-cost, simply-operated and easily-removed structure-directing templates to directly form 3D porous MnO_2 thin films on a current-collecting substrate for supercapacitor electrodes. 1D single-crystal ZnO nanowires as one of the most attractive functional semiconductor materials have been extensively studied during the past ten years. Easy availability and dissolubility even in weak acid or basic environment without damaging the coating products make ZnO nanowires be ideal structure-directing templates [11,12]. In this communication, we demonstrate a kind of new 3D porous coral-like MnO_2 nanostructure constructed on stainless steel (SS) substrates by a simple one-step ZnO-nanorod-array-mediated technique. The porous coral-like MnO_2 nanostructure thin-film SS electrode exhibits a good capacitance of 221 F g^{-1} at the 0.5 A g^{-1} with a high rate capability, and an excellent long-term cycling stability.

2. Experimental part

2.1. Synthesis of 3D porous coral-like MnO_2 on stainless steel (SS) substrate

All of chemical reagents were analytically pure and used without further purification. Firstly, ZnO nanorods were vertically grown on a piece of stainless steel according to the previous report with some modifications [13]. In Brief, firstly, freshly synthesized ZnO colloidal ethanol solution [14] was dipped on the SS and then dried by N_2 flow. The step was repeated for several times. After annealing for 10 min at 100 °C in air, the seeded SS was suspended carefully upside-down in a container containing a 100 mL aqueous solution of 0.025 M zinc nitrate hydrate ($Zn(NO_3)_2$) and 0.025 M hexamethylenetetramine (HMTA), 0.005 M polyethyleneimine (PEI, molecular weight 800 g mol^{-1} LS, Alfa Aesar), and 0.4 M ammonium hydroxide. The container was then covered and placed in a water bath at 67 °C to start the growth of ZnO nanorods. After 5 h, the SS was picked out, rinsed with copious deionized (DI) water, and then annealed in the air at 300 °C for 30 min to remove any residual organics. Secondly, the resulting SS substrate was put into a Teflon-lined stainless-steel autoclave with 25 mL capacity. Then, 20 mL of aqueous solution containing 0.1 M $KMnO_4$ and 0.05 M $MnSO_4$ was transferred to the autoclave, and heated at 180 °C for 30 min. After cooling under water flow for 10 min, the autoclave was opened. The SS substrate was picked out, rinsed with copious DI water, and then dried for 1 h at 150 °C in air. Finally, the SS substrate with a brown MnO_2 film on front surface and a pale brown film on back surface was obtained.

2.2. Structural characterization

Scanning electron microscopy (SEM) analyses were performed on a Hitachi S4800 microscope. Transmission electron microscopy (TEM) observations were carried out on a Tecnai G2 F20 U-TWIN instrument operated at 200 kV. The X-ray diffraction (XRD) data were collected using a Shimadzu X-ray diffractometer (XRD-6000) with Cu Kα radiation (λ = 0.154178 nm). X-ray photoelectron spectroscopy (XPS) spectra were measured using an ESCALab 250 electron spectrometer from Thermo Scientific Corporation.

2.3. Electrochemical measurements

Electrochemical measurements were performed on VMP3 Potentiostat/Galvanostat (EG&G, Princeton Applied Research) using a conventional three-electrode cell system. The three-electrode cell configuration consisted of a Pt foil (1.5 × 3 cm^2) as the counter electrode, a saturated calomel electrode (SCE) as the reference electrode, and the MnO_2-modified SS substrate (1 × 1 cm^2) as the working electrode. An aqueous solution of 1.0 M Na_2SO_4 served as the electrolyte at room temperature. To avoid disturbance of the MnO_2 deposited on back surface of the SS substrate without ZnO

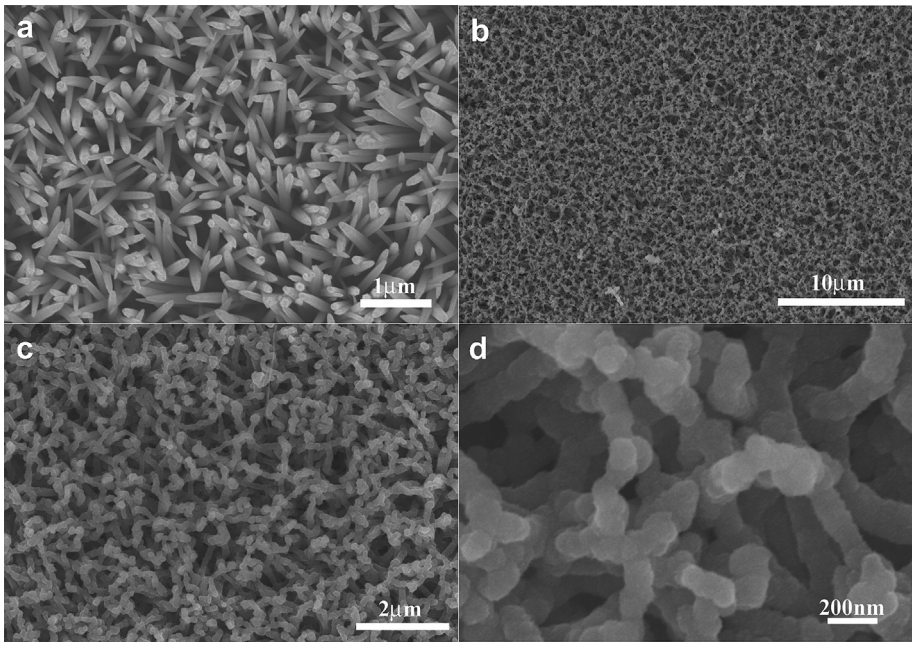

Fig. 1. Typical SEM images of (a) the ZnO nanorods on SS and (b–d) the coral-like MnO_2 in different magnifications.

nanorods, the pale brown film was removed completely by using a carbon cloth adsorbing dilute HCl solution to clean the surface before the electrochemical measurements. Cyclic voltammograms were recorded between 0 and 0.8 V (vs. SCE) at various scan rates ranging from 2 to 300 mV s^{-1}. Galvanostatic charge–discharge tests were conducted between 0 and 0.8 V (vs. SCE) at different current densities from 0.5 to 20 A g^{-1}. The electrochemical impedance spectroscopy (EIS) measurements were performed by applying an AC voltage with 5 mV amplitude in a frequency range from 0.01 Hz to 100 kHz. The specific capacitances were calculated from CV and galvanostatic charge–discharge curves respectively according to the following two equations:

$$C = \frac{\int_a^b I(V)\mathrm{d}V}{2 \times \Delta V \times \upsilon \times m} \quad (1)$$

$$C = \frac{I \times \Delta t}{\Delta V \times m} \quad (2)$$

where $\int_a^b I(V)\mathrm{d}V$ is the integrated area of CV curve in one cycle, υ is the scan rate, I is the constant discharge current, Δt is the discharging time, ΔV is the potential window, and m is the mass of the MnO_2 thin film.

3. Results and discussion

The coral-like 3D MnO_2 thin film was synthesized on preformed ZnO nanorod arrays on the SS substrate via the hydrothermal reaction between $KMnO_4$ and $MnSO_4$ solutions. The experimental details have been given above. Fig. 1a shows the typical SEM image of the ZnO nanorods grown on the SS substrate. From the image, we can observe that the ZnO nanorods grow nearly vertically on the SS substrate. Some of them slightly incline and contact with each other. The ZnO nanorods have a spear-like shape with an average diameter of ~100 nm. They can serve as ideal templates for further growing MnO_2 nanomaterials. Fig. 1b and 1c present typical SEM images of thus-obtained MnO_2 nanostructure film in different magnifications. Homogeneous coral-like MnO_2 film with porous 3D nano-architecture network was formed on the SS substrate. Further details of the network structure are shown in Fig. 1d, where many ~100 nm sized quasi-sphere aggregates were found to interconnect to construct the porous film structure. The low magnified TEM image in Fig. 2a confirms the worm or coral-like morphology of the MnO_2 nanostructures again. The high magnified TEM image in Fig. 2b reveals that the coral-like MnO_2 branches are actually composed of many small MnO_2 grains with a diameter range from 2 to 5 nm. Due to the small grain size and low weight percentage of MnO_2 in the SS substrate (~0.43% compared with SS, i.e. 0.1 mg vs. 23 mg), it is very difficult to observe the diffraction peaks of the MnO_2 nanostructure film that can be completely submerged by far strong diffraction peaks from the SS substrate in X-ray diffractogram (see Fig. S1). Therefore, the high resolution

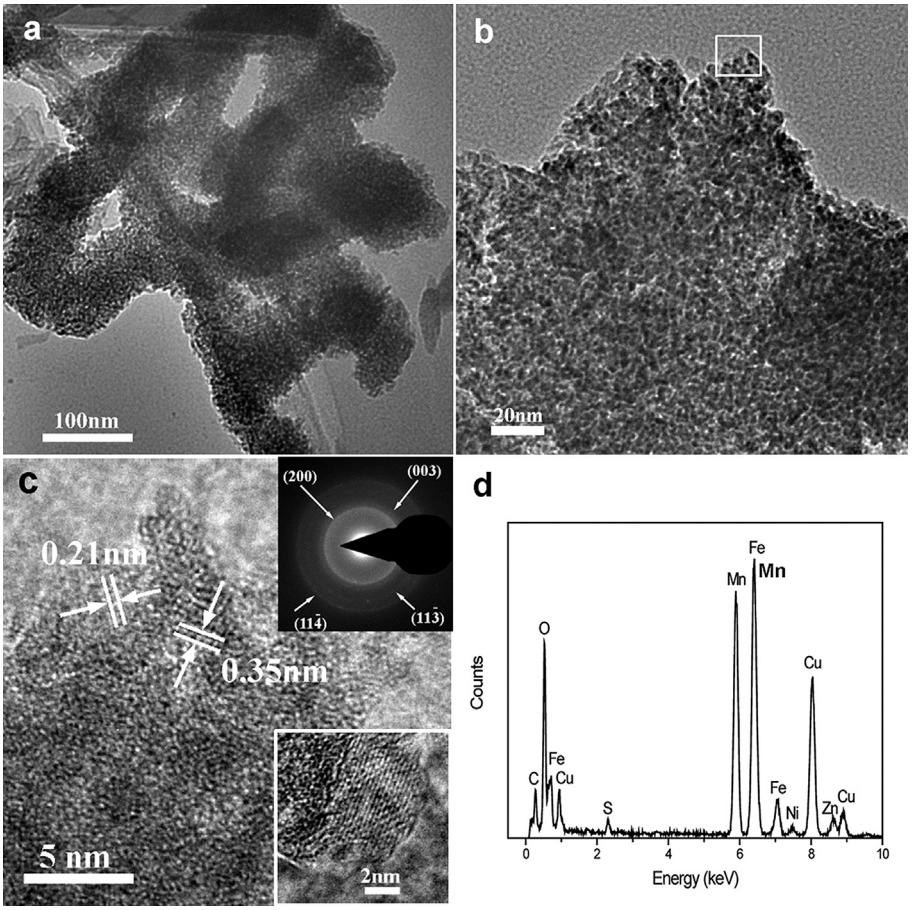

Fig. 2. (a, b) Typical TEM images of the coral-like MnO_2 under various magnifications; (c) HRTEM image of the selected area in (b), the inserts at the upper and lower right corner are the corresponding SAED pattern and typical HRTEM image of a single MnO_2 nanocrystal; (d) EDS of the sample.

TEM (HRTEM) and selected area electron diffraction (SAED) methods were used to characterize crystalline structure of the MnO_2 grains. Fig. 2c shows the HRTEM image of the selected area in Fig. 2b, where the small MnO_2 nanocrystals surrounded by amorphous interspaces are observed. Visible lattice spacing was measured to be 0.21 and 0.35 nm on two different MnO_2 grains, well matching the distance of (11-2) and (002) plane of birnessite-MnO_2 (JCPDS42-1317), respectively. For clarity, the insert at the lower right corner of Fig. 2c demonstrates a HRTEM image of a ~5 nm sized crystalline MnO_2 nanoparticle. The corresponding SAED of Fig. 2c (see the insert at upper right corner of Fig. 2c) also displays a circular diffraction pattern, a typical character of polycrystalline birnessite-MnO_2 with d-spacing values of various planes. Fig. 3d presents the energy-dispersive X-ray spectroscopy (EDS) of the sample, where the atomic ratio of O:Mn:Zn is calculated to be about 65:32:3. This shows that there is still a minute amount of ZnO existing in the MnO_2 nanostrucutures. Other elements such as C, Cu, S, Fe, Ni were also detected, which come probably from ultrathin carbon film, Cu grid, $MnSO_4$, SS substrate.

To further obtain information on the chemical composition and oxidation state of as-synthesized MnO_2 nanostructure thin-film, X-ray photoelectron spectroscopy (XPS) analysis was performed. A typical XPS survey spectrum of the thin-film is shown in Fig. S2. There are five main elements (Mn, O, Zn, Fe and C) detected on the surface of the sample, which is consistent with the EDS result. The precise region spectra for Mn2p and O1s are shown in Fig. 3a and 3b. In Fig. 3a, the Mn2p spectrum exhibits multiple splitting. Two main peaks located at 642.35 and 654.03 eV can be assigned to $Mn2p_{3/2}$ and $Mn2p_{1/2}$ of Mn^{4+} in MnO_2 respectively [4]. Meanwhile, Mn^{3+} and Mn^{5+} species were also detected in the spectrum. However, intensities of the two peaks are much weaker than that for the Mn^{4+}, implying that element Mn is present mainly in the chemical state of Mn^{4+}. In the O1s region (Fig. 3b), the broad multi-peak can be deconvoluted into three peaks at 529.93, 531.41 and 532.30 eV, corresponding to various oxygen-containing chemical states including oxide (Mn–O–Mn), hydroxide (Mn–O–H) and water (H–O–H), respectively [15].

Base on the experimental results mentioned above, a possible formation process of the unusual coral-like MnO_2 is illustrated in Fig. 4. Firstly, newly formed MnO_2 nuclei experience a rapid adsorption and aggregation on surfaces of the ZnO nanorods. To make total system energy lowest, the MnO_2 nanoparticles are inclined to form nearly spherical aggregates. With the reaction going on, the freshly generated nanoparticles are adsorbed on partial surfaces of these primary globular aggregates, making this structure grow like a creeping worm. Meanwhile, ZnO nanorods are gradually eroded by the hydrogen ions produced by a redox reaction. Finally, the slightly inclined orientation and the weaker and weaker mechanical support exerted by ZnO nanorods lead some freshly-formed coral-like MnO_2 to interlink together, forming the porous 3D nanostructure network film. It is worth mentioning that the ZnO nanorods arrays have been replaced by the coral-like MnO_2 nanostructures during the reaction process despite a little amount of ZnO still existing in the new MnO_2 nanostructures. No extra steps involving removal of the template are needed in whole process. The advantage makes the present preparation method for porous MnO_2 nanostructure be a promising technique for direct synthesis and application of 3D porous MnO_2 thin films on the conductive substrates like stainless steel and copper.

To evaluate the electrochemical performances of the 3D coral-like porous MnO_2 thin-film as a supercapacitor electrode material, we carried out cyclic voltammetry (CV) and galvanostatic charging–discharging measurements in a three-electrode system. Fig. 5a shows the typical CV curves of the sample at various scan rates ranging from 2 to 300 mV s^{-1}. The quasi-rectangular and symmetric CV curves, even at high scan rates such as 300 mV s^{-1}, indicate the MnO_2 electrode material has ideal pseudo- and reversible capacitor behaviour. Fig. 5b shows the charging–discharging curves at different current densities from 0.5 to 20 A g^{-1}. All these curves demonstrate fairly linear slopes and approximately symmetric shapes, further revealing good electrochemical reversibility and capacitive behaviour. The calculated specific capacitance as a function of current density is shown in Fig. 5c, which is comparable with the results derived from CV curves (Fig. S3). The coral-like MnO_2 nanostructure thin-film shows a high specific capacitance of 221 F g^{-1}, which is higher than the results on the basis of MnO_2 material reported by other groups, such as 3D clewlike ε-MnO_2 (120 F g^{-1}) [16], α-MnO_2 nanorods (166.2 F g^{-1}) [17] and MnO_2 nanoflowers (121.5 F g^{-1}) [18]. More significantly, the 3D porous coral-like MnO_2 thin-film not only shows a high specific capacitance but also exhibits a good rate capability. Even at a current density as high as 20 A g^{-1}, it still retains 96 F g^{-1} (about 55% of 176 F g^{-1} at 1 A g^{-1}). This result is much better than previous reports such as mesoporous MnO_2 nanowire array [19] (84 F g^{-1} at 12 A g^{-1}) and multilayer nanosheet clusters [20] (42 F g^{-1} at 50 mV s^{-1}, in comparison to 140 F g^{-1} for our result, see Fig. S3). In general, energy storage mechanism of MnO_2-based supercapacitors is suggested to originate from the ionic charge accumulation in the electric double layer existing at the electrode/electrolyte interface. In the neutral aqueous Na_2SO_4 electrolytes, the charge/discharge mechanism can be described as the following reaction:

$$MnO_2 + M^+ + e^- \leftrightarrow MnOOM \quad (3)$$

where M represents hydrated protons (H_3O^+) and/or alkali Na^+ cations. The reaction equation implies two kinds of possible

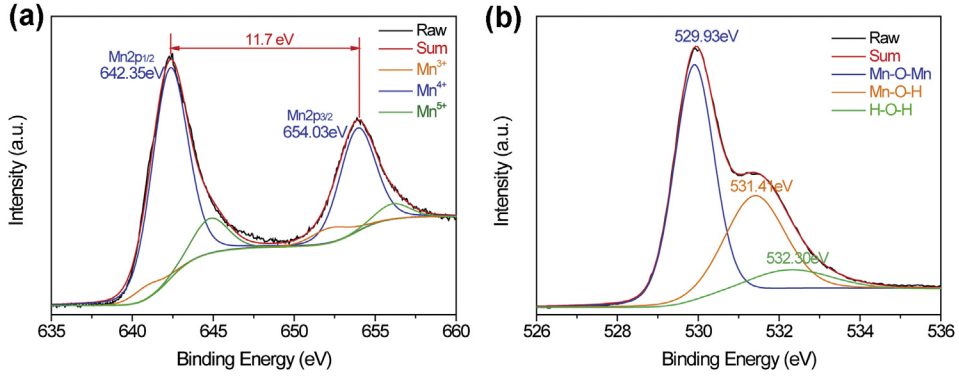

Fig. 3. XPS peaks in the regions of (a) Mn2p and (b) O1s ("Raw" represents the raw data, and "Sum" is the total fitted curve).

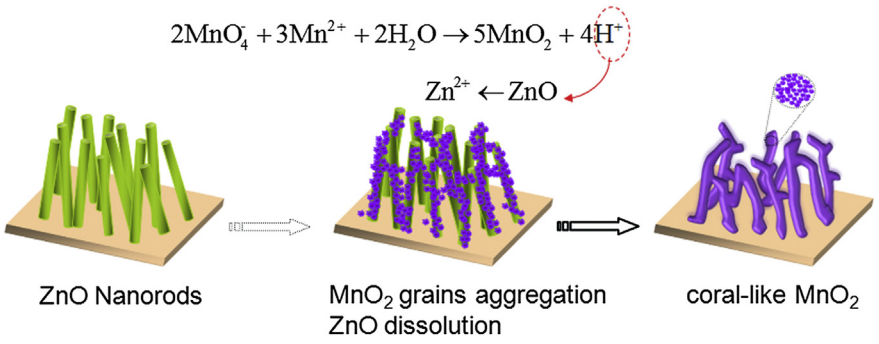

Fig. 4. A schematic illustration of a possible formation process of the coral-like porous MnO_2 nanostructure film.

processes, i.e., an adsorption/desorption process of cations at the material surface and/or an insertion/extraction process of cations into the material bulk. A recent report shows that the insertion/extraction process happens mostly on well crystallized bulk materials while the adsorption/desorption process occurs on weakly crystallized materials [21]. According to the assumption, no obvious redox waves in our CV curves imply that the charge storage process in the present coral-like porous MnO_2 nanostructure thin-film electrode system is probably mainly dominated by adsorption/desorption of cations at the nanomaterial surface with rich crystalline defects and amorphous interspaces. This is agreeable with the structure feature of the coral-like MnO_2 thin-film, as observed in the HRTEM images of Fig. 2. The high specific capacitance and excellent rate capacity of the MnO_2 thin-film can be attributed to the unique 3D porous nanostructure, which can increase the surface area of active materials, shorten the ion diffusion distance, and improve the charge-transport ability. In addition, the amorphous interspaces between the disordered MnO_2 nanocrystals may provide more accessible active sites and more effective mass transport routes. This will be beneficial for the good electrochemical performances.

The cycling stability of the MnO_2 thin-film was also examined by charge/discharge cycling at a high current density of 5 A g^{-1}, as shown in Fig. 5d. It can be clearly seen that the capacitance retention is above 100% and keep constant in the first 500 cycles. This may be caused by the gradual activation process of the porous MnO_2 aggregates [22]. After 3000 cycles, 86% of initial specific capacitance can be retained and the shape of charge–discharge curves for the last ten cycles still keeps nearly symmetric, indicating the high electrochemical stability of the coral-like MnO_2 nanostructure thin-film. The SEM examination after 3000 cycles (Fig. S4) further confirmed the structural stability of the nanostructure MnO_2.

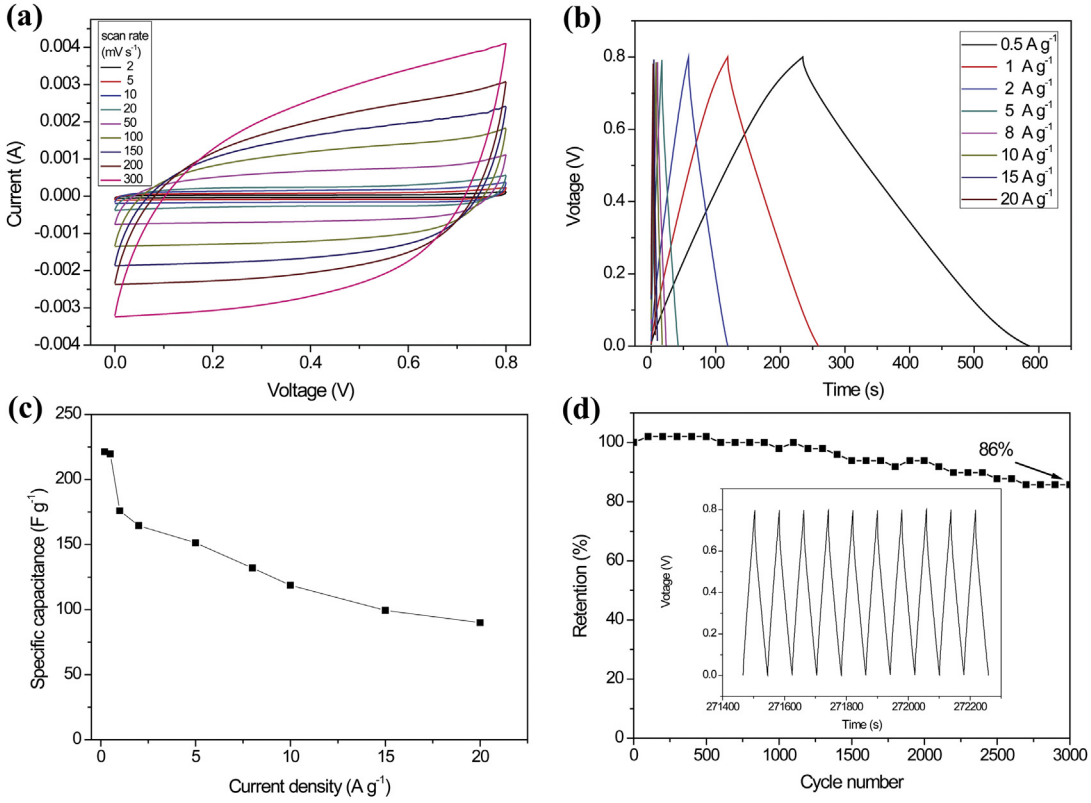

Fig. 5. (a) Typical CV curves of the coral-like MnO_2 nanostructure thin-film at different scan rates; (b) galvanostatic charge–discharge curves at various current densities; (c) the specific capacitance as a function of different current densities; (d) specific capacitance as a function of cycle number at 5 A g^{-1}, the insert shows the charge–discharge curves for last ten cycles.

4. Conclusions

In summary, a kind of 3D porous coral-like MnO_2 thin-film has been successfully synthesized directly on stainless steel by a quite simple and low-cost ZnO nanorod arrays-mediated strategy. The coral-like MnO_2 aggregates are formed by adhesion of a large amount of disorder birnessite-MnO_2 nanocrystals with a diameter range from 2 to 5 nm. This unique porous MnO_2 nanostructure thin-film exhibits a high specific capacitance, excellent rate capability and cycling stability, endowing it with a promising application in low-cost, high performance supercapacitor electrode materials.

Acknowledgements

This work was financially supported by National Basic Research Program of China (No. 2009CB930702, 2012CB933402), the Knowledge Innovation Program of the Chinese Academy of Sciences (No. KJCX2-YW-M13).

Appendix A. Supplementary data

Supplementary data related to this article can be found at http://dx.doi.org/10.1016/j.jpowsour.2013.03.176.

References

[1] J.R. Miller, P. Simon, Science 321 (2008) 651–652.
[2] P. Simon, Y. Gogotsi, Nat. Mater. 7 (2008) 845–854.
[3] G.H. Yu, L.B. Hu, N.A. Liu, H.L. Wang, M. Vosgueritchian, Y. Yang, Y. Cui, Z.N. Bao, Nano Lett. 11 (2011) 4438–4442.
[4] M. Toupin, T. Brousse, D. Belanger, Chem. Mater. 16 (2004) 3184–3190.
[5] A.S. Arico, P. Bruce, B. Scrosati, J.M. Tarascon, W. Van Schalkwijk, Nat. Mater. 4 (2005) 366–377.
[6] H. Jiang, T. Zhao, J. Ma, C.Y. Yan, C.Z. Li, Chem. Commun. 47 (2011) 1264–1266.
[7] C.L. Ho, M.S. Wu, J. Phys. Chem. C 115 (2011) 22068–22074.
[8] A.L.M. Reddy, M.M. Shaijumon, S.R. Gowda, P.M. Ajayan, J. Phys. Chem. C 114 (2010) 658–663.
[9] H.G. Zhang, X.D. Yu, P.V. Braun, Nat. Nanotechnol. 6 (2011) 277–281.
[10] B.X. Li, G.X. Rong, Y. Xie, L.F. Huang, C.Q. Feng, Inorg. Chem. 45 (2006) 6404–6410.
[11] J.P. Liu, J. Jiang, M. Bosman, H.J. Fan, J. Mater. Chem. 22 (2012) 2419–2426.
[12] J.P. Liu, Y.Y. Li, H.J. Fan, Z.H. Zhu, J. Jiang, R.M. Ding, Y.Y. Hu, X.T. Huang, Chem. Mater. 22 (2010) 212–217.
[13] C.K. Xu, P. Shin, L.L. Cao, D. Gao, J. Phys. Chem. C 114 (2010) 125–129.
[14] Z.S. Hu, G. Oskam, P.C. Searson, J. Colloid Interf. Sci. 263 (2003) 454–460.
[15] M. Chigane, M. Ishikawa, J. Electrochem. Soc. 147 (2000) 2246–2251.
[16] P. Yu, X. Zhang, D. Wang, L. Wang, Y. Ma, Cryst. Growth Des. 9 (2008) 528–533.
[17] Y. Li, H. Xie, J. Wang, L. Chen, Mater. Lett. 65 (2011) 403–405.
[18] J. Ni, W. Lu, L. Zhang, B. Yue, X. Shang, Y. Lv, J. Phys. Chem. C 113 (2008) 54–60.
[19] C. Xu, Y. Zhao, G. Yang, F. Li, H. Li, Chem. Commun. (2009) 7575–7577.
[20] Z.P. Feng, G.R. Li, J.H. Zhong, Z.L. Wang, Y.N. Ou, Y.X. Tong, Electrochem. Commun. 11 (2009) 706–710.
[21] P. Ragupathy, H.N. Vasan, N. Munichandraiah, J. Electrochem. Soc. 155 (2009) A34–A40.
[22] Z.J. Sun, H.Y. Chen, D. Shu, C. He, S.Q. Tang, J. Zhang, J. Power Sources 203 (2012) 233–242.